Taylor & Francis
Taylor & Francis Group

BRIEF REPORT

Check for updates

Endosomal-associated RFFL facilitates mitochondrial clearance by enhancing PRKN/parkin recruitment to mitochondria

Rishith Ravindran [ID][a,*], Anoop Kumar G. Velikkakath [ID][a,b,*], Nikhil Dev Narendradev [ID][a], Aneesh Chandrasekharan [ID][c], T. R. Santhoshkumar [ID][c], and Srinivasa M. Srinivasula [ID][a]

aSchool of Biology, Indian Institute of Science Education and Research Thiruvananthapuram, Kerala, India; bCentral Research Laboratory, K.S. Hegde Medical Academy, Nitte (Deemed to Be University), Karnataka, India; cCancer Research Program-1, Rajiv Gandhi Centre for Biotechnology, Kerala, India

ABSTRACT
Mutations in the ubiquitin ligase PRKN (parkin RBR E3 ubiquitin protein ligase) are associated with Parkinson disease and defective mitophagy. Conceptually, PRKN-dependent mitophagy is classified into two phases: 1. PRKN recruits to and ubiquitinates mitochondrial proteins; 2. formation of phagophore membrane, sequestering mitochondria for degradation. Recently, endosomal machineries are reported to contribute to the later stage for membrane assembly. We reported a role for endosomes in the events upstream of phase 1. We demonstrate that the endosomal ubiquitin ligase RFFL (ring finger and FYVE like domain containing E3 ubiquitin protein ligase) associated with damaged mitochondria, and this association preceded that of PRKN. RFFL interacted with PRKN, and stable recruitment of PRKN to damaged mitochondria was substantially reduced in *RFFL* KO cells. Our study unraveled a novel role of endosomes in modulating upstream pathways of PRKN-dependent mitophagy initiation.

Abbreviations CCCP: carbonyl cyanide 3-chlorophenylhydrazone; DMSO: dimethyl sulfoxide; EGFP: enhanced green fluorescence protein; KO: knockout; PRKN: parkin RBR E3 ubiquitin protein ligase; RFFL: ring finger and FYVE like domain containing E3 ubiquitin protein ligase; UQCRC1: ubiquinol-cytochrome c reductase core protein 1; WT: wild-type

Introduction

Stringent quality control mechanisms ensure organelle and cellular homeostasis. Signaling pathways that regulate mitochondrial quality and function are believed to play critical roles in diverse physiological processes including cell survival and their dysregulation results in the development of numerous pathological conditions like neurological disorders, cancer and myopathies [1–3]. Macroautophagy/autophagy is a conserved intracellular catabolic process in which cytoplasmic contents, including damaged mitochondria, are sequestered in double-membrane autophagosomes and delivered to the lysosomal compartment for degradation [4]. Selective elimination of dysfunctional and damaged mitochondria involving autophagic machinery and lysosomes is known as mitophagy [5].

Though cells can employ various other cellular tools like ESCRT (the endosomal sorting complex required for transport) machinery [6], MDVs (mitochondrial derived vesicles) [7,8] etc., to remove mitochondrial contents, mitophagy mediated by PINK1 (PTEN induced kinase 1) and PRKN (parkin RBR E3 ubiquitin protein ligase) is relatively well studied [9–11]. In depolarized mitochondria, PINK1 accumulated on the outer mitochondrial membrane phosphorylates PRKN, which in turn pleiotropically ubiquitinates several mitochondrial proteins result in the clearance of

mitochondria by mitophagy [12]. However, details of the sequence of events involved in the PRKN recruitment, stability and identities of the proteins functioning in this pathway are not clear.

However, recent reports suggest a role for endosomes and endosomal proteins in mitochondrial clearance. Crosstalk of endosomal related proteins RABGEF1, RAB5, MON1-CCZ1 complex, and RAB7A result in ATG9A (autophagy related 9A) vesicle recruitment to phagophore assembly site [13]. Moreover, RAB5-positive endosomes have been implicated in the elimination of damaged mitochondria via the ESCRT complex machinery, and contribute to cytoprotective roles against oxidative stress [6,14]. It has also been proposed that RAB11A endosomes enable the autophagy of damaged mitochondria [15]. How endosomes influence the mitochondrial quality and the crosstalk between the endosomal machinery and the above molecules that are known to be critical for mitophagy, remain to be elucidated.

RFFL/CARP2 (ring finger and FYVE like domain containing E3 ubiquitin protein ligase), is one of the two RING and FYVE-like domain containing proteins in the human genome. While the RING domain confers ubiquitin ligase activity, the FYVE-like motif along with its N-terminal sequence is reported to associate with phospholipids like

phosphatidylinositol-3-phosphate [16]. Interestingly, RFFL-positive vesicles are also reported to be positive for RAB5, RAB7, RAB9, RAB11, and LAMP1 (lysosomal associated membrane protein 1) markers of diverse endocytic vesicles [17–19]. In this study, we report that RFFL-positive vesicles associated with damaged mitochondria and contributed to mitochondrial elimination by facilitating PRKN recruitment.

Results

Endosomal ubiquitin ligase RFFL associated with damaged mitochondria

Because the endosomal machinery has been reported to contribute to mitophagy, we investigated the role of RFFL-positive endosomes in mitochondrial elimination. For these studies, we have used cells stably expressing RFFL cloned under a weak promoter using a retroviral vector [20]. As a first step, we monitored the association between RFFL endosomes and damaged mitochondria using confocal microscopy of A549 lung carcinoma cells stably expressing RFFL-EGFP. In these cells, mitochondria were stained with MitoTracker Red CMXRos. As expected, in cells treated with DMSO, RFFL-EGFP was primarily localized to intracellular vesicles, which are reported to be positive for various known endosomal markers [19]. In these cells, mitochondria appeared mostly as filamentous structures, with a minimum association with RFFL vesicles (Figure 1(a)). However, in cells treated with the mitochondrial uncoupler CCCP mitochondria were found to be fragmented as expected, with substantial numbers being surrounded by RFFL vesicles (Figure 1(a)). Line scan analysis demonstrated clear encircling of damaged mitochondria by RFFL (Figure 1(b) lower panel), with nearly 60% of the live cells showing a positive association between these organelles within 25 min of treatment (Figure 1(c)). Mander's coefficient analysis from individual cells also showed a significant correlation of RFFL on mitochondria upon CCCP treatment (Figure 1(d)). Similar association of RFFL with damaged mitochondria was observed in cells sorted for low RFFL-EGFP expression (Figure S1A, B). The expression level of RFFL-EGFP in these cells assessed by immunoblotting showed protein levels not too high, but closer to the endogenous expression (Figure S1C). Another mitochondrial uncoupler commonly used is valinomycin. Results from cells treated with valinomycin also showed a similar association with what was observed in cells treated with CCCP (Figure S1D).

The association of RFFL vesicles with damaged mitochondria was further analyzed by super-resolution imaging (structured illumination microscopy [SIM]) in cells stably expressing EBFP2-Mito-7, RFFL-mRFP and YFP-PRKN (Figure 1(e)). The encirclement of damaged mitochondria by RFFL-positive vesicles was also noted in 3D super-resolution SIM images (Figure 1(f) and Video S1). Association of PRKN with mitochondria in cells is shown in Figure S1E. To further demonstrate association between mitochondria and RFFL vesicles, the RFFL-EGFP vesicles were precipitated from cellular extracts prepared without detergent using GFP Trap and immuno-probed for mitochondrial protein UQCRC1

(ubiquinol-cytochrome c reductase core protein 1). Consistent with association noted in CCCP treated cells between RFFL and mitochondria, more UQCRC1 protein was observed upon CCCP treatment (Figure 1(g)).

To understand whether the association between RFFL and mitochondria occurs in a cell-type independent manner, we have explored the association of RFFL with mitochondria using neuronal cell line Neuro-2a (N2a), as mitochondrial quality maintenance is known to be critical for neuronal cell homeostasis [21,22]. For this, we generated N2a cells stably expressing RFFL-mRFP. As it was noted in A549 cells, RFFL appeared to associate with intracellular vesicles in N2a cells as well (Figure S1F). In N2a cells also very little (basal level) association was noted between RFFL and mitochondria (MitoTracker Deep Red FM) under untreated conditions. However, as observed in CCCP treated A549 cells, a significant colocalization between RFFL-mRFP and damaged mitochondria was noted in N2a cells (Figure S1F, G). A similar association was also observed in other cell lines like human embryonic kidney cells, HEK293T and osteosarcoma cell line, U2OS (data not shown), suggesting that RFFL association with damaged mitochondria is cell-type independent.

RFFL-associated mitochondria are positive for RAB7A and RAB5B

Studies have shown that some of the endosomes or endosomal proteins involve in the regulation of PRKN mediated mitochondrial clearance [6,13,15,23]. Hence, we investigated whether RFFL-positive vesicles that are associated with mitochondria are also positive for known mitophagy-linked endosomal markers, namely RAB5 and RAB7. Both RAB5 and RAB7 are widely used as markers to identify endosomes, and RFFL is known to associate with intracellular vesicles that are positive for these endosomal markers [18,19]. Towards this end, we have transiently transfected RFFL-mRFP stably expressing N2a cells with GFP-RAB5B or GFP-RAB7A and stained the mitochondria with MitoTracker Deep Red FM. Without any treatment, very little colocalization was noted between RFFL-positive RAB7A or RAB5B vesicles and mitochondria. However, in CCCP treated cells numerous RFFL-positive RAB5B or RAB7A vesicles were found to be in association with mitochondria (Figure 2(a-d)). Quantification of the percentage of cells with RFFL and RAB7A or RAB5B localized to mitochondria are shown in Figure 2(e,f). Moreover, to demonstrate association of RFFL or RAB7A vesicles with mitochondria, the GFP-RAB7A vesicles were enriched from extracts of cells expressing GFP-RAB7A along with RFFL-mRFP, prepared without detergent using GFP Trap and immuno-probed for mitochondrial protein UQCRC1. Consistent with association noted in CCCP treated cells between RFFL, RAB7A and mitochondria, more UQCRC1 and RFFL-mRFP was observed upon CCCP treatment (Figure 2(g)). These results collectively demonstrate that RFFL-RAB7A or RAB5B endosomes are associated with damaged mitochondria.

As RFFL vesicles associated with the mitochondria along with RAB7A, we were interested in exploring whether absence
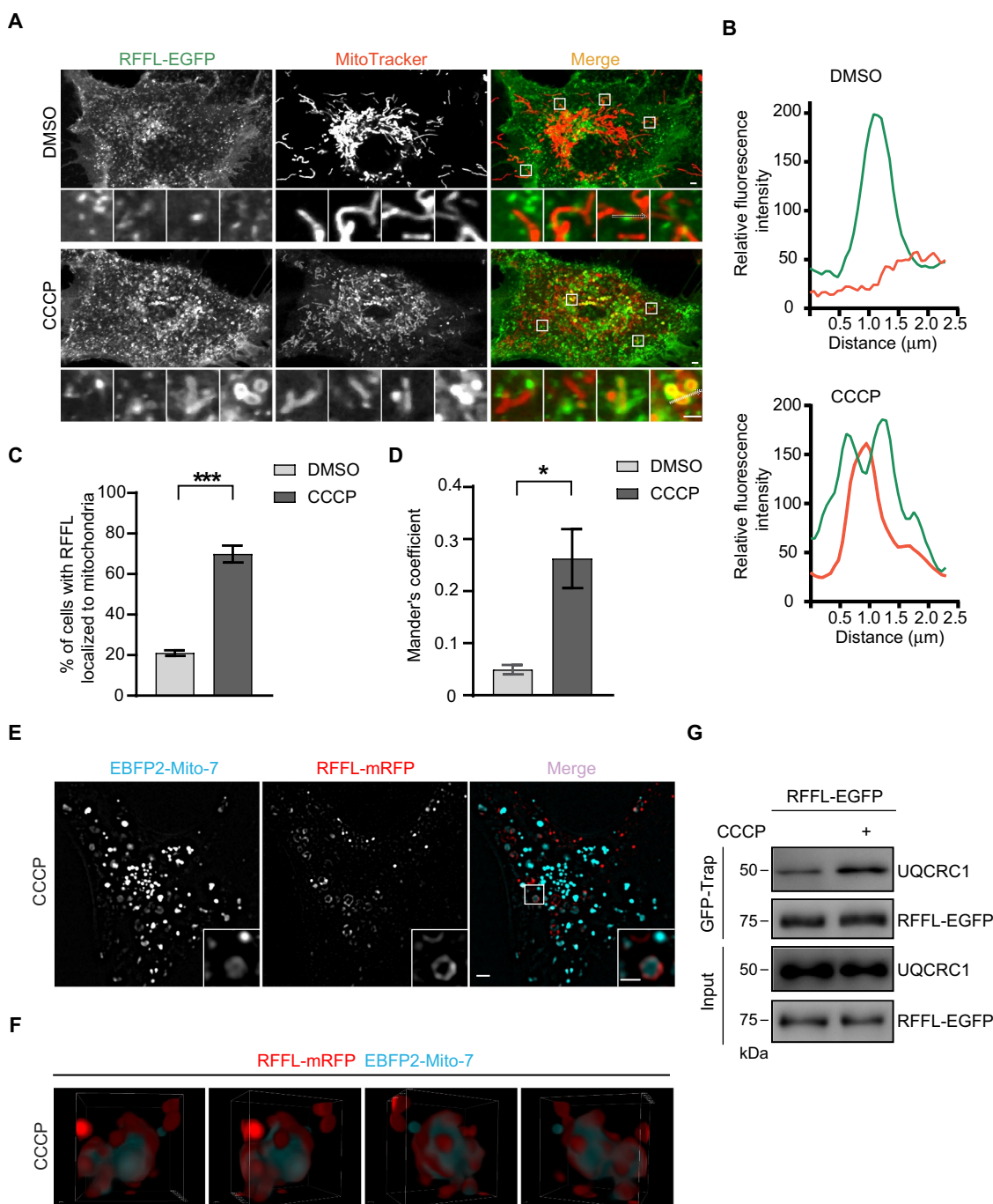
Figure 1. Endosomal ubiquitin ligase RFFL localized with damaged mitochondria. (a) A549 cells stably expressing RFFL-EGFP stained with MitoTracker Red CMXRos for 30 min, were washed with DMEM followed by treatment with DMSO or 20 μM CCCP. Images of live cells were taken during 10–25 min of CCCP treatment. Scale: 2 μm; inset scale: 1 μm. (b) Line scan analyzes of the area under the arrow are shown. (c) Percentage of cells with RFFL-EGFP-positive mitochondria (MitoTracker Red CMXRos) was quantified manually (cells having more than four RFFL localized on MitoTracker were considered for counting). (d) The localization of RFFL with mitochondria is represented by Mander's coefficient from individual cells. Error bars represent mean ± SEM in cases of c and d from three independent experiments with a minimum of 50 cells per experiment. Statistical significance was calculated using a two-tailed unpaired t-test. P-values are <0.0001 in the case of c, and 0.0204 in case of d. (E) U2OS cell line stably expressing EBFP2-Mito-7 and RFFL-mRFP along with YFP-PRKN (See Figure S1E) were treated with 20 μM CCCP and images of live cells were captured using super-resolution microscopy at 14 h post-treatment. Scale: 2 μm; inset scale: 1 μm. (f) Super-resolution 3D still images in four different angles of EBFP2-Mito-7-positive mitochondria and RFFL-mRFP-positive endosomes shown as a video (Video S1). (g) GFP-positive vesicles from A549 cells stably expressing RFFL-EGFP treated with either DMSO or 10 μM CCCP for 3.5 h were enriched using GFP-Trap and probed with indicated antibodies.

of RFFL can affect recruitment of endosomes to the mitochondria. To investigate such an idea, we generated *RFFL* KO cells using the CRISPR-Cas9 system and used three independent colonies (#2, 9 and 12) in our experiments. All three clones were validated using western blotting (Figure S2A). Though endosomes that are positive RFFL and RAB7A were found to be in association with mitochondria, absence of RFFL did not significantly impair recruitment of RAB7A vesicles to mitochondria as observed in *RFFL* KO cells (Figure S2B).

We further examined the dynamics of the association between endosomes and damaged mitochondria using time-

Figure 2. RFFL-localized mitochondria are positive for RAB7A and RAB5B. (a and b) Neuro-2a cells stably expressing RFFL-mRFP were transiently transfected with either GFP-RAB7A (a) or GFP-RAB5B (b). After 18 h of transfection, cells were stained with MitoTracker Deep Red FM for 30 min and were subsequently treated with 10 μM CCCP. Images of live cells from 10 to 40 min after CCCP treatment or untreated (UT) are shown. Yellow outlined arrows point to localization between RFFL (pseudo green color) and RAB7A or RAB5B (pseudo blue color) without mitochondria. Filled white arrows point to localization between RFFL (pseudo green color), Mitochondria (pseudo red color) and RAB7A or RAB5B (pseudo blue color). Filled yellow arrows point to localization between RFFL (pseudo green color) and Mitochondria (pseudo red color) without RAB5B. Scale: 2 μm; inset scale: 1 μm. (c and d) Percentage of RFFL-positive vesicles per cell that localized with either RAB7A (c) or RAB5B (d) with or without mitochondria was quantified manually. Error bars represent mean ± SEM in cases of C and D from three independent experiments with a minimum of 35 cells per experiment. (e and f) The graph represents the percentage of cells showing localization of mitochondria with RAB7A (e) or RAB5B (f) and RFFL (cells having more than four RFFL and RAB7A or RAB5B localized on MitoTracker were considered for counting). Error bars represent mean ± SEM in cases of e and f from three independent experiments with a minimum of 50 cells per experiment. Statistical significance was calculated using a two-tailed unpaired t-test. P-values are <0.0001 in the case of e and f. (g) GFP-positive vesicles from HEK293T cells stably expressing RFFL-mRFP and transiently transfected with GFP-RAB7A, treated with either DMSO or 10 μM CCCP for 3.5 h were enriched using GFP-Trap and probed with indicated antibodies.

lapse live imaging microscopy over a period of 12 min. Monitoring of cells stably expressing RFFL-EGFP and stained with MitoTracker Red CMXRos revealed the formation of protrusions of GFP-positive structures from RFFL vesicles towards damaged mitochondria (Figure S2C and Video S2), which transiently hover around mitochondria. To further understand this phenomenon, we have used a photobleaching strategy. A549 cells stably expressing RFFL-EGFP were exposed to bleaching using 488 nm Argon laser at a region of interest, consisting of RFFL-positive mitochondria. After bleaching, the movement of RFFL vesicles (green) in the vicinity of damaged mitochondria (red) was monitored for a period of 2 min. As early as 41s after photobleaching, movement of GFP-positive structures from the surrounding area of the bleached region towards the damaged mitochondria was noted (Figure S2D, Video S3). As pointed by arrows, these structures appeared tubular in nature. Moreover, under these conditions, within 2 min the mitochondria were noted to be surrounded with multiple RFFL-positive vesicles, suggesting a plausible role for RFFL-positive endosomes in mitophagy. As these findings suggest that the RFFL endosomes are associated with mitochondria, the role of RFFL association with damaged mitochondria and PRKN, a well-known E3 involved in the elimination of damaged mitochondria, is explored further.

RFFL associated with damaged mitochondria prior to PRKN, and RFFL KO cells showed defective PRKN recruitment

Because PRKN is known to regulate mitophagy, we investigated the function of RFFL in PRKN-mediated mitophagy. We monitored the localization of RFFL and PRKN in CCCP treated A549 cells, stably expressing RFFL-EGFP or YFP-PRKN individually and pre-stained with MitoTracker Red CMXRos. As shown in Figure 3(a), RFFL localization to mitochondria was observed within 10 min of treatment, whereas that of PRKN was noted only after 30 min (Figure 3(b)). To investigate whether the kinetics of recruitment of both these proteins to mitochondria is specific to A549 cells, or similar pattern can be observed in other cells, we stably expressed both RFFL-mRFP and YFP-PRKN simultaneously in U2OS cell line. Simultaneous expression of these proteins also helped to monitor their relative recruitment vs mitochondria. As seen in A549 cells, RFFL recruitment to mitochondria was found in early time points compared to PRKN recruitment. Surprisingly, very little colocalization between mitochondria that associates with RFFL and PRKN were noted (Figure 3(c)). Time-course measurements indicated maximum localization of RFFL within 10 min, whereas PRKN peaked after 30 min (Figure 3(d)). However, proximity between RFFL- (arrowheads) and PRKN-positive (arrows) mitochondria were observed, without overt localization (Figure 3(c), 50 min CCCP).

As RFFL is localized to the mitochondria prior to PRKN, we were interested in exploring RFFL function in regulating PRKN recruitment to the mitochondria. We monitored the status of PRKN localization to damaged mitochondria by immunostaining for TOMM20 (translocase of outer mitochondrial membrane 20) and GFP in A549 cells, WT or *RFFL* KO stably expressing YFP-PRKN. In DMSO-treated cells, as expected, YFP-PRKN remained cytosolic in both WT and *RFFL* KO cells (Figure S3A). In CCCP-treated WT cells, YFP-PRKN appeared as punctate structures that are positive for the TOMM20, indicating its localization to damaged mitochondria. In *RFFL* KO cells, however, a significant reduction in YFP-PRKN localized to mitochondria was noted with most of the PRKN remained diffused in the cytosol though the total amount of mitochondria in *RFFL* KO cells appeared similar to that found in WT (Figure S3A, B). While differences in PRKN localization was significant up to 1 h and at 6 h of CCCP treatment, the differences were less pronounced during 2 h to 4 h suggesting a delay both in the recruitment and stabilization of PRKN on the mitochondria (Figure S3A, B) in *RFFL* KO cells. These observations from *RFFL* KO cells (clone # 2) were not a result of the off-target effect, as we could observe this phenotype in two other independent *RFFL* KO clones # 9 and 12 (Figure S3C). For all other experiments, *RFFL* KO clone # 2 was used. To further validate this phenotype, we enriched PRKN from extracts of WT and *RFFL* KO cells expressing YFP-PRKN using GFP Trap and the precipitates were probed for endogenous RFFL and UQCRC1. Consistent with the imaging data, more UQCRC1 was noted in CCCP-treated WT than KO cells (Figure S3D). In membrane fractions consisting of mitochondria represented by UQCRC1, isolated from CCCP treated WT and *RFFL* KO cells, more YFP-PRKN was noted from WT than from KO (Figure S3E). These data collectively suggest a plausible role of RFFL in PRKN recruitment to mitochondria.

Endosomal-association-defective RFFL variant failed to associate with mitochondria and affected PRKN recruitment

RFFL, in addition to the ubiquitin ligase domain, consists of two cysteine residues (C5, 6) that are predicted to be involved in palmitoylation (Figure 4(a)). Both these cysteines are required for the endosomal association as RFFL^{C5,6A} variant is unable to localize to intracellular vesicles (Figure 4(b) and [19,24]). To understand whether ubiquitin ligase activity and/or endosomal localization are required for the association of RFFL with damaged mitochondria, we have reconstituted A549 *RFFL* KO cells with EGFP tagged RFFL variants. The reconstituted cells were stained with MitoTracker Red CMXRos, and the association of various RFFL mutant variants with damaged mitochondria was assessed after CCCP treatment. Interestingly, RFFL ubiquitin ligase inactive mutant (RFFL^{H333A}) also showed colocalization with damaged mitochondria after CCCP treatment. The RFFL^{H333A} association with mitochondria appeared to be similar to that noted with WT RFFL with some differences. WT RFFL formed a distinct ring-like pattern around the damaged mitochondria, which was not apparent in the case of the RFFL^{H333A} (Figure 4(b)). These results suggest that ubiquitin ligase activity is not essential for RFFL association with mitochondria.

Unlike WT RFFL and RFFL^{H333A} that localized to intracellular vesicles, endosomal localization defective RFFL variant
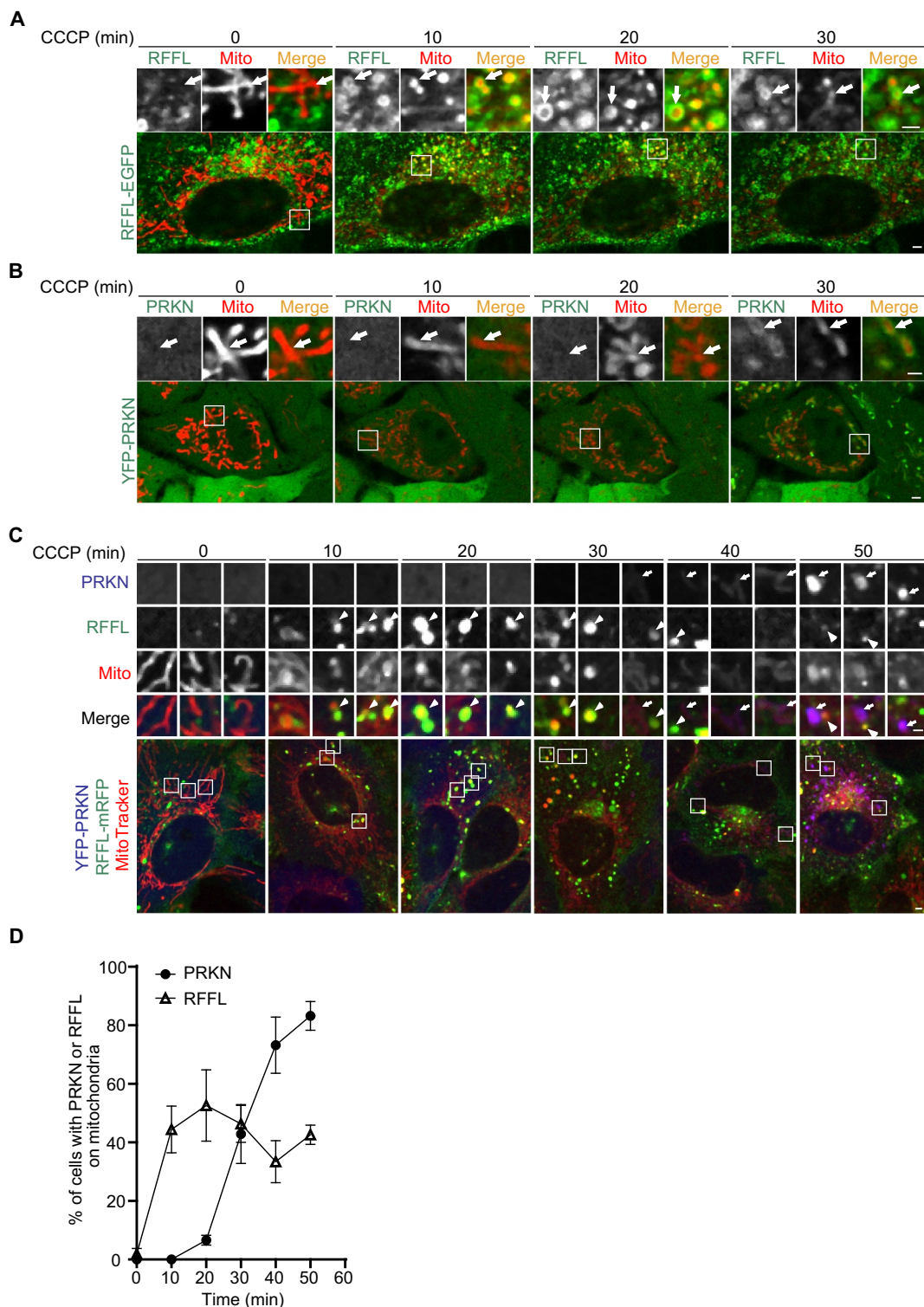
Figure 3. RFFL localized with damaged mitochondria before PRKN. (a and b) A549 cells stably expressing RFFL-EGFP (a) or YFP-PRKN (b) stained with MitoTracker Red CMXRos for 30 min were washed in DMEM followed by treatment with 20 μM CCCP. Images of live cells at the indicated time points after treatment are shown. Scale: 2 μm; inset scale: 1 μm. (c) U2OS cells stably expressing RFFL-mRFP and YFP-PRKN were pre-stained with MitoTracker Deep Red FM for 30 min and washed with DMEM. These cells were subsequently treated with 20 μM CCCP. Images of live cells at the indicated time points after treatment are shown. Localization between PRKN (pseudo blue) and Mitochondria (pseudo red) was shown with arrows. Localization between RFFL (pseudo green) and Mitochondria (pseudo red) are shown with arrowheads. Scale: 2 μm; inset scale: 1 μm. (d) The graph represents the percentage of cells with mitochondria localized with either RFFL-EGFP or YFP-PRKN (cells having more than four RFFL or PRKN localized on MitoTracker were considered for counting) at indicated time points. Data shown is from three independent experiments and a minimum of 50 cells were counted per experiment. Error bars represent mean ± SEM.

(RFFL[C5,6A]) showed a diffuse cytosolic pattern. Moreover, in CCCP treated cells, the RFFL[C5,6A] showed very little detectable association with damaged mitochondria (Figure 4(b)).

Quantification of the percentage of cells with RFFL variants on mitochondria is included in Figure 4(e). These observations suggest cysteine residues are essential for RFFL

association with damaged mitochondria. To investigate the effect of palmitoylation on RFFL association with mitochondria, we have used a known palmitoylation inhibitor, 2-bromohexadecanoic/palmitic acid (2-BP). 2-BP is known to act as an inhibitor for the protein acyltransferases (PATs), thus inhibiting palmitoylation of proteins [25,26]. Treatment with 2-BP, showed a reduction in CCCP-induced RFFL association with the damaged mitochondria compared to untreated cells (Figure S4A, B). These results suggest a yet to be determined role for palmitoylation in mitophagy.

Next, to understand whether the association of RFFL with mitochondria is required for PRKN recruitment, we have generated *RFFL* KO cells reconstituted with untagged versions of WT RFFL, or RFFL^H333A or RFFL^C5,6A along with YFP-PRKN. These cells were stained with MitoTracker CMXRos, and PRKN localization was observed in DMSO- and CCCP- treated conditions. As expected, PRKN appeared as a diffused cytosolic pattern with no association with MitoTracker in all the cells after DMSO treatment (Figure S4C). Whereas upon CCCP-treatment, *RFFL* KO cells expressing either WT RFFL or RFFL^H333A showed an increase of PRKN recruitment compared to the *RFFL* KO cells, but similar to WT cells (Figure 4(c,f)), *RFFL* KO cells reconstituted with RFFL^C5,6A showed a pattern similar to that noted in *RFFL* KO alone cells (Figure 4(d-g)). These results suggest the importance of RFFL association with mitochondria for PRKN recruitment. Interestingly, these results also point out that RFFL facilitates PRKN recruitment to the damaged mitochondria independent of its ligase activity. However, RFFL requires N-terminal cysteine residues, which are important for recruiting PRKN to damaged mitochondria.

RFFL interacted with PRKN and regulated mitophagy independent of its ubiquitin ligase activity

Since the data indicated that RFFL facilitates PRKN recruitment to the mitochondria, we investigated whether RFFL can interact with PRKN. To explore such an idea, we have transfected HEK293T cells with cDNA constructs of *PRKN* and *WT RFFL* or *RFFL*^H333A mutant with appropriate controls. The cellular lysates were used to immunoprecipitate RFFL using RFFL specific antibody and the immunoprecipitates were probed for PRKN. In comparison to the control samples, we were able to consistently see the presence of PRKN in the precipitates from WT RFFL samples. Surprisingly, the amount of PRKN pulled was much more in the precipitates from the lysates of cells overexpressing ligase inactive mutant than of WT RFFL though the amount of RFFL present in both WT and mutant samples were similar (Figure 5(a)). As these results suggested that RFFL can interact with PRKN, to further validate the same, we have performed the immunoprecipitation of endogenous RFFL in A549 cells stably expressing YFP-PRKN. Consistent with the data from overexpression, in untreated cells, very little basal level of interaction between endogenous RFFL and PRKN was noted. Moreover, after CCCP treatment, a noticeably more amount of PRKN was observed in the immunoprecipitates of RFFL, suggesting

an increased association between these proteins in treated cells (Figure 5(b)). This interaction is specific, as no PRKN band was detected in immunoprecipitates from the lysates of CCCP-treated *RFFL* KO cells (Figure 5(b)). The interaction was further validated by FLIM analysis using YFP-PRKN and RFFL-mRFP (Figure S4D, E).

As RFFL can interact with PRKN and facilitates PRKN recruitment to the mitochondria, we were interested to know whether RFFL promotes PRKN ubiquitination. For this, we have accessed the extent of ubiquitination in PRKN precipitates from lysates of A549 cells, WT and *RFFL* KO stably expressing YFP-PRKN with or without CCCP treatment. PRKN was immunoprecipitated from the cell lysates using PRKN-specific antibody, and the precipitates were probed separately with PRKN antibody and anti-Ub antibody. The amount of PRKN that was precipitated remained more or less the same in all the samples. Under DMSO treated conditions, the amount of polyubiquitination on PRKN pull-down from both WT and KO cells remained the same. As expected, an increase in polyubiquitination was observed upon CCCP treatment in WT cells, whereas this increase was substantially reduced in cell lysates that do not express RFFL (Figure 5(c)), suggesting that RFFL contributes to the ubiquitination of PRKN under CCCP-treated conditions. To investigate whether the increased polyUb signal in PRKN immunoprecipitate is indeed on PRKN, we have transfected HEK293T cells with cDNAs of RFFL variants or PRKN along with HA-Ub. The extent of polyubiquitination on PRKN was assessed by performing immunoprecipitation under denaturation conditions using PRKN specific antibody. In DMSO treated conditions, PRKN was found to be substantially more polyubiquitinated in the presence of WT RFFL compared to the empty vector control and the ligase inactive mutant. Notwithstanding a substantial increase in the extent of polyubiquitinated PRKN upon CCCP treatment from control cells, a noticeable enhancement in polyubiquitination was observed in WT RFFL expressing cells (Figure 5(d)). These results collectively suggest that RFFL can interact with PRKN and promotes its polyubiquitination.

As we found that RFFL vesicles surrounded damaged mitochondria and influenced PRKN recruitment to mitochondria, we investigated the role of RFFL in the elimination of mitochondria. For this, we monitored levels of two mitochondrial proteins, UQCRC1, an IMM (inner mitochondrial membrane)/matrix protein or TIMM23 (translocase of inner mitochondrial membrane 23), an IMM protein [27,28] with or without CCCP treatment in A549 cells. Consistent with the report of elimination of the mitochondria upon CCCP treatment [27], a significant decrease in the levels of UQCRC1 and TIMM23 was noted in WT cells. Importantly, the extent of reduction of both these proteins were much less in the absence of RFFL, i.e., in *RFFL* KO cells after 24 h of CCCP treatment, suggesting that RFFL contributes to the elimination of damaged mitochondria (Figure 5(e)). This reduction was similar to that observed in *ATG5* KO cells (Figure 5(e)), where PRKN-dependent mitophagy is known to be ineffective [9]. To further validate the role of RFFL in PRKN mediated
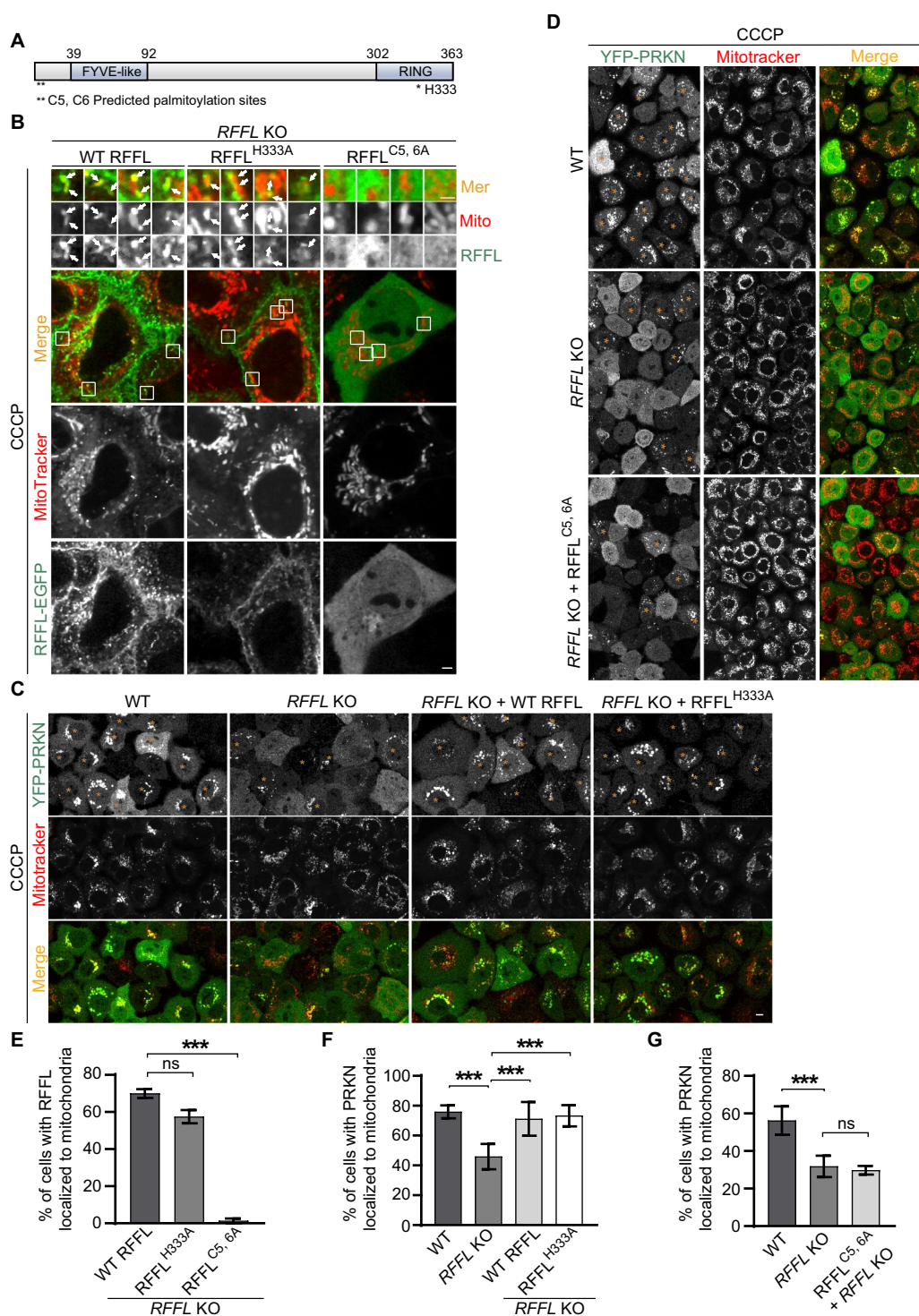
Figure 4. Endosomal-localization-defective RFFL variant failed to localize with mitochondria and affects PRKN recruitment. (a) Schematic representation of human RFFL protein with predicted palmitoylation sites (* denotes cysteines at 5th and 6th positions) and a conserved histidine residue at 333rd position in the RING domain. (b) A549 *RFFL* KO cells expressing EGFP tagged WT RFFL, or RFFL[H333A], or RFFL[C5,6A] mutant, were pre-stained with MitoTracker Red CMXRos. These cells were washed with DMEM and subsequently treated with 20 μM CCCP. Representative images of live cells over 10–40 min of treatment are shown. White arrows show the localization of RFFL with mitochondria. Inset contrast was adjusted for better visibility. Scale: 2 μm; inset scale: 1 μm. (c and d) A549 cells stably expressing YFP-PRKN in WT, or *RFFL* KO, or *RFFL* KO reconstituted with untagged WT RFFL, or RFFL[H333A] or RFFL[C5,6A], were pre-stained with MitoTracker Red CMXRos for 30 min. These cells were washed with DMEM and subsequently treated with 10 μM CCCP. Representative images of live cells at 6 h (5.5 h to 6.5 h) of treatment are shown. Orange asterisks represent cells counted as positive for PRKN on mitochondria. Scale: 5 μm. (e) The bar graph shows the percentage of cells with more than four RFFL-EGFP puncta localized to MitoTracker. Error bars represent mean ± SEM from three independent experiments. a minimum of 50 cells were counted for each experiment. Statistical significance was determined using ordinary one-way ANOVA followed by Tukey's multiple comparisons test. P-values for WT RFFL vs RFFL[H333A] is 0.1063 and for WT RFFL vs RFFL[C5,6A] is <0.0001. (f and g) Bar graph showing the percentage of cells with at least fifteen YFP-PRKN puncta localized to MitoTracker during this period. Data shown are from three independent experiments and a minimum of 75 cells were counted per experiment. Error bars represent mean ± SEM. Statistical significance was calculated using ordinary one-way ANOVA followed by Tukey's multiple comparisons test. P-values for *RFFL* KO vs WT is < 0.0001 (in case of f), *RFFL* KO vs *RFFL* KO + WT RFFL is 0.0006, *RFFL* KO vs *RFFL* KO + RFFL[H333A] is 0.0003, *RFFL* KO vs WT is 0.0001 (in case of g), and *RFFL* KO vs *RFFL* KO + RFFL[C5,6A] is 0.9321.
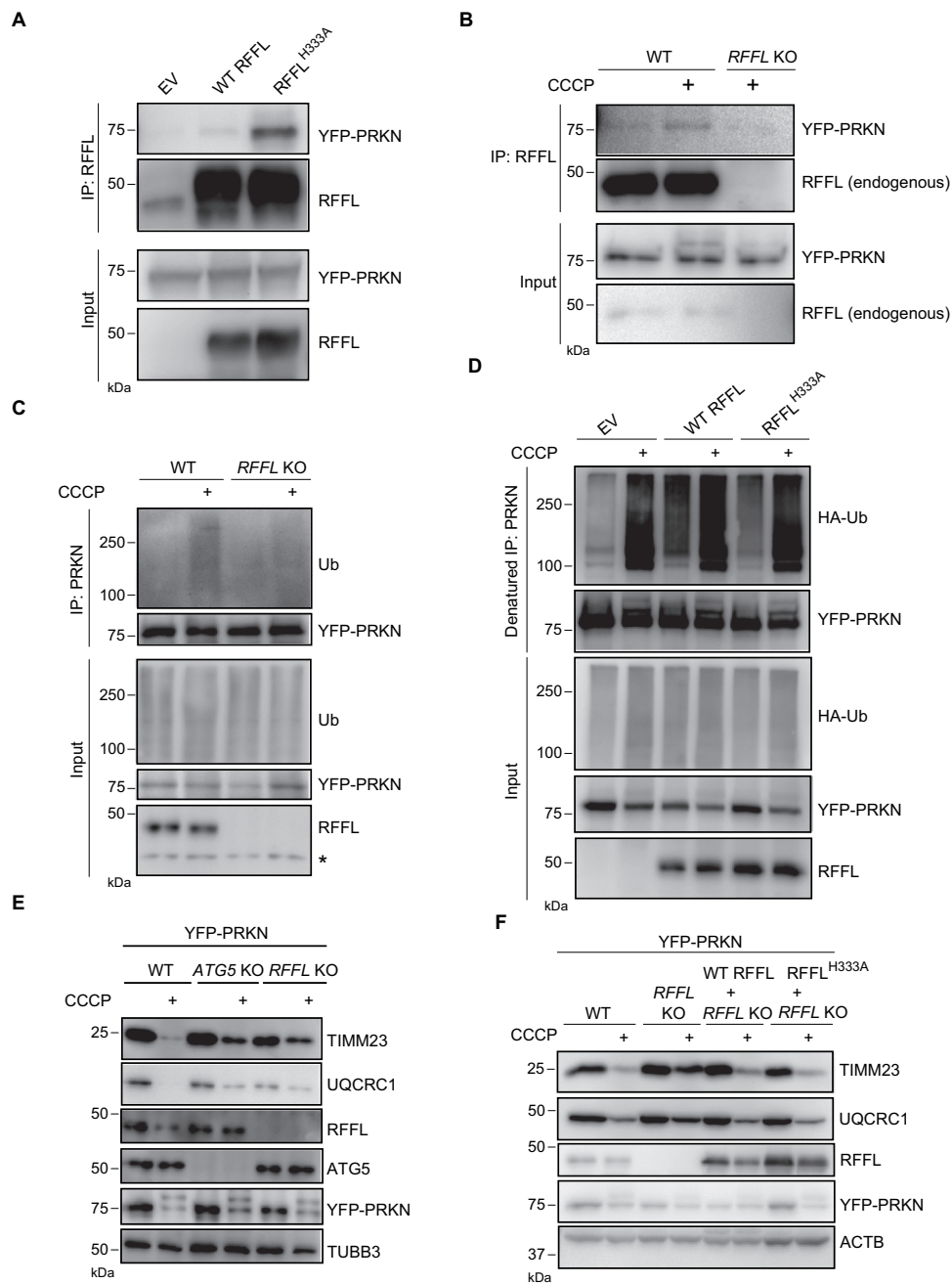
Figure 5. RFFL interacted with PRKN and regulated mitophagy independent of its ubiquitin ligase activity. (a) HEK293T cells transfected with empty vector (EV) or Flag tagged *WT RFFL* or *RFFL*[H333A] were transiently cotransfected with *YFP-PRKN*. Cells were lysed and RFFL was immunoprecipitated using RFFL specific antibody. The precipitates and lysates were probed with indicated antibodies. (b) A549 cells, WT or *RFFL* KO cells stably expressing YFP-PRKN were treated with either DMSO or 10 µM CCCP for 3 h. Cells were lysed and endogenous RFFL was immunoprecipitated using RFFL specific antibody. The precipitates and lysates were probed with indicated antibodies. (c) A549 cells, WT or *RFFL* KO stably expressing YFP-PRKN were treated with DMSO or 10 µM CCCP for 3 h. Cells were lysed and YFP-PRKN was immunoprecipitated using PRKN specific antibody. The precipitates and lysates were probed with indicated antibodies. * denotes a non-specific band. (d) HEK293T cells transiently transfected with empty vector (EV) or WT RFFL or H333A along with HA-Ub and YFP-PRKN were treated with DMSO or 10 µM CCCP for 3 h. Cells were lysed and YFP-PRKN was immunoprecipitated using a PRKN specific antibody under denaturation conditions. The precipitates and lysates were probed with indicated antibodies. (e) A549 cells (WT or *ATG5* KO or *RFFL* KO) stably expressing YFP-PRKN were treated with DMSO or 20 µM of CCCP for 24 h. The cell lysates were subjected to western blotting with the indicated antibodies. (f) A549 cells, WT or *RFFL* KO, or *RFFL* KO reconstituted with untagged WT RFFL or RFFL[H333A] stably expressing YFP-PRKN were treated with DMSO or 10 µM of CCCP for 24 h. The cell lysates were subjected to immunoblotting with the indicated antibodies.

clearance of damaged mitochondria, we have monitored the levels of UQCRC1 or TIMM23 in *RFFL* KO A549 cells reconstituted with WT or ligase inactive mutant. Concomitant with the normal PRKN recruitment to mitochondria observed in these cells (Figure 4(c)), expression of both WT and ligase inactive mutant rescued the degradation of mitochondrial proteins, TIMM23 and UQCRC1 (Figure 5(f)). Quantification of data from these immunoblots is presented as Figure S4F. These results collectively indicate the crosstalk between endosomal ubiquitin ligase RFFL and cytosolic ubiquitin ligase PRKN in the clearance of damaged mitochondria.

Discussion

Endosomes are believed to provide membranes for the autophagosomes and regulate autophagy [29]. Emerging evidence envisages important roles for endosomal-associated proteins in the mitochondrial clearance by lysosomes via ESCRT pathway or PRKN-mediated mitophagy [6,13,23]. Post-translational modification with ubiquitin (ubiquitination) mediated by ubiquitin ligases like PRKN plays critical roles in maintaining mitochondrial homeostasis. PRKN association with mitochondria involves PINK1, and the PINK1 and PRKN feedforward loop-generated phospho-Ub facilitates activation and multimerization or stabilization of PRKN on mitochondria [10,30,31]. Notwithstanding very little is known of the mechanisms that facilitate PRKN, which is uniformly distributed in the cytosol, translocation to the damaged mitochondria. Our study proposes a novel mechanism on how endosomes/endosomal associated molecules regulate PRKN recruitment and elimination of damaged mitochondria. In this study, we demonstrated that RFFL-associated endosomes surround damaged mitochondria. We provide evidence that a variant of RFFL, (RFFL^{C5,6A}) that is deficient in its endosomal localization was unable to associate with mitochondria. Moreover, we found that mitochondria-associated with RFFL vesicles were also positive for RAB7A, or to a lesser extent RAB5B, that represent different endosomal vesicles. Collectively, these results indicated that it is the RFFL endosomal vesicles, not RFFL molecules that associate with damaged mitochondria. The mechanism(s) by which RFFL-endosomes sense damaged mitochondria and move towards organelle needs to be explored.

Another exciting aspect of RFFL association with mitochondria is that it was observed as early as 10 min of CCCP treatment, prior to PRKN translocation to mitochondria. Moreover, both RFFL- and PRKN-positive mitochondria appeared as distinct populations with very few mitochondria exhibiting association with both RFFL and PRKN at the same time. However, it was also noted that several of the RFFL- and PRKN-positive vesicles were in close proximity. The existence of distinct mitochondrial populations based on membrane potential and PRKN translocation are reported earlier [9]. We believe that these discrete populations represent different, but yet connected stages, of organelle disintegration that are reported during mitophagy [7,32,33]. These results, along with the observation of compromised PRKN recruitment in *RFFL* KO cells, led us to propose (Figure S5A) that the association of RFFL vesicles with the mitochondria prime these organelles for PRKN recruitment and this process involves separation of RFFL vesicles with some mitochondrial content. Indeed, sequential RFFL and PRKN recruitment that were observed in CCCP treated cells (Figure S5B and Video S4) supports such a model.

We also provide evidence that RFFL can interact with and facilitate the ubiquitination of PRKN in CCCP-treated cells. Interestingly, the ligase activity of RFFL was not required for interaction with PRKN or the recruitment of later to and elimination of mitochondria. Such an E3-independent role in autophagy is not limited to RFFL alone. Other ubiquitin ligases, namely TRIM13 (tripartite motif containing 13) and SMURF1 (SMAD specific E3 ubiquitin protein ligase 1), that regulate autophagy are reported to function independently of their respective ubiquitin ligase activities [34,35]. Smurf1 in addition to HECT's domain that confers ubiquitin ligase activity also possesses a phospholipid-binding C2 domain that anchors to membrane phospholipids and functions in protein targeting to the subcellular compartments [36]. While Smurf1 regulates mitophagy independent of its E3 ligase activity, its C2 domain is required for the same. Similar to Smurf1, RFFL is an ubiquitin ligase with a FYVE-like domain, that is believed to bind to phospholipid molecules with the help of post-translational modifications such as palmitoylation [16,24]. RFFL has been shown to be palmitoylated [24], and the sites for this modification are predicted to be Cysteine residues in positions 5 and 6. RFFL^{C5,6A} not only failed to associate with damaged mitochondria but also was unable to rescue PRKN translocation to the mitochondria in *RFFL* KO cells. Though both RFFL and Smurf1 function independent of their E3 ligase activity, they require domains that are responsible for lipid binding to regulate mitophagy, suggesting both these proteins might work in a similar fashion in regulating mitophagy. As recycling endocytic vesicles are shown to contribute to autophagosome formation and mitophagy [15], more studies in this area further our understanding of the biogenesis of autophagosomes in PRKN-mediated mitophagy.

Interestingly independent of its mitophagic role, PRKN is also reported to effect calcium homeostasis. PRKN overexpression in cardiac specific tissues results in hypertrophy, pulmonary edema, and ventricular dysfunction compared to WT mice. In these cells PRKN localizes to the sarcoplasmic reticulum and alter calcium homeostasis via PLN (phospholamban) demonstrating adversarial effect of higher PRKN protein level [37]. In this context our observation of PRKN ubiquitination and a reduction in its level, independent of mitophagy, under RFFL overexpression conditions can be of significance in maintaining optimal PRKN level in cells. PRKN-RFFL interactions might also have implications in physiological processes other than mitophagy and would be interesting for further investigations.

An important role of RFFL in mitophagy is further supported by reports of modulation of PRKN recruitment to mitochondria and its activity by two other molecules TP53 (tumor protein p53) and MDM2 [38,39], though many details of this process remain unknown. Importantly, both TP53 and MDM2 are interacting partners of RFFL [40]. Further investigations are required to exactly understand roles played by RFFL vs MDM2 or TP53 in mitophagy.

This study also opens many important aspects for further studies. How does RFFL-endosomes sense damaged mitochondria and the role of PINK1 in RFFL recruitment to damaged mitochondria? Another important issue that warrants further exploration is the role of RFFL in PRKN independent mitophagy and whether RFFL-positive mitochondrial vesicles are linked to events in the scheme of piecemeal mitophagy that is believed to occur at the physiological level. More studies are needed to understand the nature and function of RFFL-positive mitochondrial vesicles. This study with RFFL would further unravel the contribution of

endosomes to PRKN-dependent mitophagy. The role for RFFL-positive endosomes may not be limited to mitophagy, but might also extend to various other fields of autophagy like aggrephagy, pexophagy, reticulophagy, xenophagy, nucleophagy and zymophagy.

Materials and methods

Cell culture and generation of stable cell lines

All cells were maintained in Dulbecco's modified Eagle's medium (Thermo Fisher Scientific, 10569-010) containing 10% heat-inactivated FBS (Thermo Fisher Scientific, 10270–106) and 1% penicillin-streptomycin (HiMedia, A001A) in a 5% CO_2 incubator at 37°C. For inducing mitochondrial damage, 80–85% of confluent cells were treated with Carbonyl cyanide-m-chlorophenylhydrazone (CCCP) (Sigma-Aldrich, C-2759) or Valinomycin (Sigma-Aldrich, V0627) after 18 h of plating. 2-bromohexadecanoic acid (Sigma-Aldrich, 21604) were treated 30 min prior to CCCP treatment. Mitochondria were stained with 100 nM of either MitoTracker Red CMXRos (Thermo Fisher Scientific, M7512) or MitoTracker Deep Red FM (Thermo Fisher Scientific, M22426) for 30 min in culture media followed by one wash in DMEM before CCCP treatment. To develop U2OS cells stably expressing YFP-PRKN and EBFP2-Mito-7, initially, the cells were transfected with YFP-PRKN and stable cells were generated by selection using G418 (Sigma-Aldrich, A1720). The stably expressing cells were further transfected with EBFP2-Mito-7 and cells expressing both the transgene were sorted using flow cytometer sorter equipped with a 375 nm laser for EBFP excitation (BD Biosciences FACS Aria III, USA). Multiple clones were expanded after further selection in G418 for two weeks, and stably expressing clones were used for the current study. Cells stably expressing RFFL-EGFP were generated as per the previous protocol [19]. Briefly, HEK293T cells were transfected with pMYsIP-RFFL-EGFP along with pCAG-VSVG and pUMVC plasmids using Lipofectamine 3000 reagent (Thermo Fisher Scientific, L3000-015). Four days post-transfection, cell supernatants were harvested and were incubated with A549 or U2OS cells in the presence of 4 μg/mL polybrene (Sigma-Aldrich, H9268). Cells were cultured in puromycin (1 μg/mL; Sigma-Aldrich, P8833) containing DMEM for selection. Other stable cell lines mentioned were also prepared using a similar protocol.

Plasmids and antibodies

Human RFFL cDNA (NCBI reference sequence: NM_001017368.2:141–1232) or YFP-PRKN [9] with indicated mutations and tags were cloned to pMYs-IP for stable cell line generation [20]. pFLAG-CMV2 WT RFFL and RFFL[H333A] was a gift from Wafik S. El-Deiry [16]. Following constructs used were received from Addgene: YFP-Parkin (PRKN) was a gift from Richard Youle (23955) [9], GFP-RAB5B (61802) and GFP-RAB7A (61803) were a gift from Gia Voeltz [41], EBFP2-Mito-7 was a gift from Michael Davidson (55248) [42], pCAG-VSVG was a gift from Arthur Nienhuis and Patrick Salmon (35616), pUMVC was a gift from Bob

Weinberg (8449) [43], PX458 was a gift from Feng Zhang (48138) [44]. The following antibodies were used in this study, anti-RFP (ChromoTek, 5f8-100), anti-RFFL (generated in our laboratory), anti-GAPDH (Abgenex, 10–10011), anti-ACTB (Elabscience, E-AB-20058), anti-TUBB3 (Elabscience, E-AB-20070), anti-ATG5 (Cell Signaling Technology, 12994 T), anti-UQCRC1 (Thermo Fisher Scientific, 16D10AD9AH5), anti-TIMM23 (Santa Cruz Biotechnology, sc-514463), anti-GFP (Clontech, 632375), anti-GFP (Thermo Fisher Scientific, A6455), anti-PRKN (Santa Cruz Biotechnology, sc-32282), anti-ubiquitin (Ub; Santa Cruz Biotechnology, sc-8017), anti-mouse HRP (Thermo Fisher Scientific, 61–6520), anti-rabbit HRP (Thermo Fisher Scientific, 65–6120), anti-rat HRP (Jackson ImmunoResearch, 712–035-150), anti-mouse light chain specific HRP (Jackson ImmunoResearch, 115–035-174), anti-rabbit light chain specific HRP (Jackson ImmunoResearch, 211–032-171).

Western blotting

18 h after plating, cells at 80–85% confluency were washed and pelleted at 850 × g in ice-cold PBS (Thermo Fisher Scientific, 18912014). Cell lysis was done in ice for 30 min using lysis buffer containing 50 mM Tris-Cl, pH 7.5 (Sigma-Aldrich, T6066), 150 mM sodium chloride (Sigma-Aldrich, S3014), 1% Triton X-100 (Sigma-Aldrich, X100), 1 mM EDTA, pH 8 (Sigma-Aldrich, E5134), 1 mM phenylmethyl-sulfonyl fluoride (Sigma-Aldrich, P7626) and 1X protease inhibitor cocktail (Sigma-Aldrich, P8340). The supernatant was collected after centrifuging the lysate at 13500 × g for 10 min at 4°C. Total protein levels in the supernatant were normalized using BCA (Thermo fisher Scientific, 23225). Samples were mixed with 5X Laemmli buffer containing 250 mM Tris-Cl, pH 6.8, 10% SDS (Sigma-Aldrich, L3771), 30% glycerol (Sigma-Aldrich, G9012), 5% 2-mercaptoethanol (Sigma-Aldrich, M6250), 0.02% bromophenol blue (HiMedia, MB123), and heated for 10 min at 95°C before loading them into SDS-PAGE. Samples separated in SDS-PAGE were later transferred to the PVDF membrane (Merck, IPVH00010). Immunoblot analysis was performed by using antibodies as indicated. They were visualized with chemiluminescent HRP substrate (Merck, WBKLS0500). Signal intensities were calculated using Quantity One version 4.6.9.

Immunoprecipitation

Cell extracts were prepared in IP buffer containing 20 mM Tris-Cl, pH 7.6, 150 mM sodium chloride, 5 mM EGTA (Sigma-Aldrich, 03777), 0.5% Triton X-100, 1 mM phenyl-methylsulfonyl fluoride, 1X protease inhibitor cocktail (Sigma-Aldrich P8340, and 04693159001), 1X phosphatase inhibitor cocktail (Sigma-Aldrich, P5726 and P0044), and 100 mM N-ethylmaleimide (Sigma-Aldrich, E3876). Lysates were then incubated with RFFL antibody at 4°C for 6 h. The RFFL or PRKN protein complex was then pulled down by incubating antibody-containing lysate with protein A or G agarose beads (Santa Cruz Biotechnology, sc-2001 or sc-2002) at 4°C for 1 h. Agarose beads were suspended in

Laemmli buffer and heated at 95°C in all samples or at 37°C in the case of PRKN IP samples. Immunoprecipitation under denaturation condition was performed by lysing the cells at 90°C for 10 min in lysis buffer containing 10 mM Tris-Cl, pH 7.6, 1% SDS, 5 mM EDTA, 10 mM DTT (Sigma-Aldrich, D0632), 1 mM phenylmethylsulfonyl fluoride, 1X protease inhibitor cocktail, 1X phosphatase inhibitor cocktail, and 100 mM N-ethylmaleimide. The lysate was then diluted 10 times with the IP buffer and Immunoprecipitation was performed as mentioned above.

Enrichment of GFP-positive vesicles and subcellular fractionation

GFP-positive vesicles were enriched using an earlier protocol with some modifications [45]. In brief, cells were harvested in ice-cold PBS in 500 × g for 5 min. Pellet were then homogenized by passing through 26-gauge needle 25 times in buffer containing 10 mM Tris-Cl, pH 7.5, 250 mM sucrose (Sigma-Aldrich, S0389), 1 mM phenylmethylsulfonyl fluoride and 1X protease inhibitor cocktail (Sigma-Aldrich, P8340). Supernatant was then incubated and processed with the GFP-Trap agarose beads (ChromoTek, gta-20) to obtain the GFP-positive vesicles as per manufacturer protocol.

Subcellular fractionation was performed as described previously [46] with a few modifications. Briefly, cells were harvested ice cold PBS followed by the resuspension in homogenization buffer (HB) containing 250 mM sucrose, 20 mM HEPES/KOH, pH 7.5 (Sigma-Aldrich, H4034), 10 mM KCl (Sigma-Aldrich, P9541), 1.5 mM $MgCl_2$ (Sigma-Aldrich, 208337), 1 mM EDTA, 1 mM EGTA, 1 mM phenylmethylsulfonyl fluoride, and 1X protease inhibitor cocktail (Sigma-Aldrich, P8340). Cells were then lysed in HB by 12 passages through 26-gauge needle syringe and centrifuged at 500 × g for 2 min at 4°C to obtain nuclear or un-lysed cell pellet and post-nuclear supernatant (PNS). PNS was further centrifuged at 10,000 × g for 10 min at 4°C to obtain heavy membrane (HM) fraction in pellet and post membrane fraction in the supernatant.

CRISPR KO preparation

A549 cells were transfected with PX458 containing *RFFL* or *ATG5* gRNAs using Lipofectamine 3000 and sorted for GFP-positive cells after 3 days of transfection using flow cytometry. Later, cells were serially diluted and plated in 96 wells to grow single colonies. *RFFL* KO or *ATG5* KO from each clone was confirmed using western blot. Sequences of gRNA used are as follows: *RFFL* 5'-GGTGGAACCATGCTGGAGTG-3' and *ATG5* 5'-AACTTGTTTCACGCTATATC- 3' [35].

Live cell imaging and immunocytochemistry

Live cell imaging was performed after 18 h of plating of cells in glass-bottom dishes (MatTek Corporation, P35G-1.0–20-C). Fourteen to 18 h of CCCP were chosen for time-lapse, photobleaching experiments and super-resolution imaging because early hours of CCCP showed the dynamic movement of RFFL vesicles which made the capture of RFFL-

mitochondria population and photobleaching technically difficult. These movements were slower at later hours of CCCP. Glass bottom dishes were placed into an on-stage incubator with 5% CO_2 and 37°C. For immunocytochemistry, cells were grown on coverslips and fixed in 4% paraformaldehyde (PFA) for 14 min. Permeabilization was done in 0.1% Triton X-100 for 10 min followed by blocking in 3% BSA for 30 min. Cells were then incubated with anti-GFP (Thermo fisher Scientific, A-6455) and anti-TOMM20 antibodies (Santa Cruz Biotechnology, sc-17764) followed by incubating with respective secondary fluorophore-conjugated antibodies; Alexa Fluor 488 donkey anti-rabbit (Thermo Fisher Scientific, A-21206) and Alexa Fluor 568 goat anti-mouse (Thermo Fisher Scientific, A-11031). After the antibody incubation, cells were mounted on a glass slide with ProLong Gold antifade reagent (Thermo Fisher Scientific, P36930). Images were acquired using Leica TCS SP5 II (Leica Microsystem, Wetzlar, Germany) laser scanning inverted confocal microscope with oil-immersion objectives (HCX PL APO CS 63.0 × 1.40 OIL UV or HCX PL APO CS 100.0 × 1.40 OIL). Photobleaching was carried out using a 488 nm argon laser at 80% laser power on a chosen ROI (region of interest). Representative confocal images used for figure preparation were noise reduced using LAS AF median filtering, keeping the same settings for all samples. Unprocessed images were used for all quantifications. Super-resolution imaging was carried out using structured illumination microscopy (3D-SIM), N-SIM (Nikon, Tokyo, Japan). Cells grown in a glass-bottom dish were at 5% CO2 with 37°C using an on-stage incubator from Tokai Hit (Japan). Cells were imaged using 100 × 1.49 maintained NA oil immersion objective. Images were taken using EMCCD Camera iXon 897 (Andor, USA) were reconstructed using NIS elements software following standard protocol.

Statistical analysis

Data were collected from at least three independent experiments. Significance levels were set at = 0.05. *$P < 0.05$, **$P < 0.01$, and ***$P < 0.001$. All statistical analyzes were performed in GraphPad Prism (Version 8.3.1).

ORCID

Rishith Ravindran http://orcid.org/0000-0002-5093-9652
Anoop Kumar G. Velikkakath http://orcid.org/0000-0002-3863-918X
Nikhil Dev Narendradev http://orcid.org/0000-0002-5641-3571
Aneesh Chandrasekharan http://orcid.org/0000-0001-6045-3739
T. R. Santhoshkumar http://orcid.org/0000-0003-3386-7105
Srinivasa M. Srinivasula http://orcid.org/0000-0003-4804-6916

References

[1] Arun S, Liu L, Donmez G. Mitochondrial biology and neurological diseases. Curr Neuropharmacol. 2015;14(2):143–154.

[2] Ahuja AS. Understanding mitochondrial myopathies: a review. PeerJ. 2018;2018:(5)

[3] Porporato PE, Filigheddu N, Pedro JMBS, et al. Mitochondrial metabolism and cancer. Cell Res. 2018;28(3):265–280.

[4] Dikic I. Proteasomal and autophagic degradation systems. Annu Rev Biochem. 2017;86(1):193–224.

[5] Montava-Garriga L, Ganley IG. Outstanding questions in mitophagy: what We Do and Do Not Know. J Mol Biol. 2020;432(1):206–230.

[6] Hammerling BC, Najor RH, Cortez MQ, et al. A Rab5 endosomal pathway mediates Parkin-dependent mitochondrial clearance. Nat Commun. 2017;8(1):8.

[7] Sugiura A, McLelland G-L, Fon EA, et al. A new pathway for mitochondrial quality control: mitochondrial-derived vesicles. EMBO J. 2014;33(19):2142–2156.

[8] McLelland GL, Lee SA, McBride HM, et al. Syntaxin-17 delivers PINK1/parkin-dependent mitochondrial vesicles to the endolysosomal system. J Cell Biol. 2016;214(3):275–291.

[9] Narendra D, Tanaka A, Suen DF, et al. Parkin is recruited selectively to impaired mitochondria and promotes their autophagy. J Cell Biol. 2008;183(5):795–803.

[10] Narendra DP, Jin SM, Tanaka A, et al. PINK1 is selectively stabilized on impaired mitochondria to activate Parkin. PLoS Biol. 2010;8(1):e1000298.

[11] Durcan TM, Fon EA. The three 'P's of mitophagy: PARKIN, PINK1, and post-translational modifications. Genes Dev. 2015;29(10):989–999.

[12] Pickles S, Vigié P, Youle RJ. Mitophagy and Quality Control Mechanisms in Mitochondrial Maintenance. Current Biology; 2018. R170–R185.

[13] Yamano K, Wang C, Sarraf SA, et al. Endosomal rab cycles regulate parkin-mediated mitophagy. eLife. 2018;7:1–32.

[14] Hsu FS, Spannl S, Ferguson C, et al. Rab5 and Alsin regulate stress-activated cytoprotective signaling on mitochondria. eLife. 2018;7:1–37.

[15] Puri C, Vicinanza M, Ashkenazi A, et al. The RAB11A-Positive compartment is a primary platform for autophagosome assembly Mediated by WIPI2 recognition of PI3P-RAB11A. Dev Cell. 2018;45(1):114–131.e8.

[16] McDonald ER, El-Deiry WS. Suppression of caspase-8- and −10-associated RING proteins results in sensitization to death ligands and inhibition of tumor cell growth. Proceedings of the National Academy of Sciences of the United States of America. 2004;101 (16):6170–6175.

[17] Coumailleau F, Das V, Alcover A, et al. Over-expression of Rififylin, a new RING finger and FYVE-like domain-containing protein, inhibits recycling from the endocytic recycling compartment. Mol Biol Cell. 2004;15 (10):4444–4456.

[18] Liao W, Xiao Q, Tchikov V, et al. CARP-2 Is an Endosome-Associated Ubiquitin Ligase for RIP and Regulates TNF-Induced NF-κB activation. Current Biology. 2008;18 (9):641–649.

[19] Okiyoneda T, Veit G, Sakai R, et al. Chaperone-Independent peripheral quality control of CFTR by RFFL E3 ligase. Dev Cell. 2018;44(6):694–708.e7.

[20] Kitamura T, Koshino Y, Shibata F, et al. Retrovirus-mediated gene transfer and expression cloning: powerful tools in functional genomics. Exp Hematol. 2003;31(11):1007–1014.

[21] Rugarli EI, Langer T. Mitochondrial quality control: a matter of life and death for neurons. EMBO J. 2012;31(6):1336–1349.

[22] Ma K, Chen G, Li W, et al. Mitophagy, mitochondrial homeostasis, and cell fate. Front Cell Dev Biol. 2020;8(June):1–14.

[23] Heo JM, Ordureau A, Swarup S, et al. RAB7A phosphorylation by TBK1 promotes mitophagy via the PINK-PARKIN pathway. Sci Adv. 2018;4(11):1–18.

[24] Araki K, Kawamura M, Suzuki T, et al. A palmitoylated RING finger ubiquitin ligase and its homologue in the brain membranes. J Neurochem. 2003;86(3):749–762.

[25] Flannery AR, Czibener C, Andrews NW, et al. Palmitoylation-dependent association with CD63 targets the Ca2+ sensor synaptotagmin VII to lysosomes. J Cell Biol. 2010;191 (3):599–613.

[26] Jennings BC, Nadolski M, Ling Y, et al. 2-Bromopalmitate and 2-(2-hydroxy-5-nitro-benzylidene)-benzo[b]thiophen-3-one inhibit DHHC-mediated palmitoylation in vitro. J Lipid Res. 2009;50 (2):233–242.

[27] Yoshii SR, Kishi C, Ishihara N, et al. Parkin mediates proteasome-dependent protein degradation and rupture of the outer mitochondrial membrane. J Biol Chem. 2011;286 (22):19630–19640.

[28] Klionsky DJ, Abdelmohsen K, Abe A, et al. Guidelines for the use and interpretation of assays for monitoring autophagy (3rd edition). Autophagy. 2016;12(1):1–222.

[29] Tooze SA, Abada A, Elazar Z. Endocytosis and autophagy: exploitation or cooperation? Cold Spring Harb Perspect Biol. 2014;6 (5):1–15.

[30] Wauer T, Simicek M, Schubert A, et al. Mechanism of phospho-ubiquitin-induced PARKIN activation. Nature. 2015;524(7565):370–374.

[31] Ordureau A, Sarraf SA, Duda DM, et al. Quantitative proteomics reveal a feedforward mechanism for mitochondrial PARKIN translocation and ubiquitin chain synthesis. Mol Cell. 2014;56 (3):360–375.

[32] McLelland GL, Goiran T, Yi W, et al. Mfn2 ubiquitination by PINK1/parkin gates the p97-dependent release of ER from mitochondria to drive mitophagy. eLife. 2018;7:1–35.

[33] Twig G, Elorza A, Molina AJA, et al. Fission and selective fusion govern mitochondrial segregation and elimination by autophagy. EMBO J. 2008;27(2):433–446.

[34] Tomar D, Singh R, Singh AK, et al. TRIM13 regulates ER stress induced autophagy and clonogenic ability of the cells. Biochim Biophys Acta Mol Cell Res. 2012;1823(2):316–326.

[35] Orvedahl A, Sumpter R, Xiao G, et al. Image-based genome-wide siRNA screen identifies selective autophagy factors. Nature. 2011;480(7375):113–117.

[36] Lu K, Li P, Zhang M, et al. Pivotal role of the C2 domain of the smurf1 ubiquitin ligase in substrate selection. J Biol Chem. 2011;286(19):16861–16870.

[37] Shires SE, Lampert MA, Kubli DA, et al. Abstract 45: the dark side of Parkin: the toxic effects of enhanced parkin levels. Circ Res. 2016;119(suppl_1). DOI:10.1161/res.119.suppl_1.45.

[38] Hoshino A, Mita Y, Okawa Y, et al. Cytosolic p53 inhibits Parkin-mediated mitophagy and promotes mitochondrial dysfunction in the mouse heart. Nat Commun. 2013;4(1):1–12.

[39] Kook S, Zhan X, Thibeault K, et al. Mdm2 enhances ligase activity of parkin and facilitates mitophagy. Sci Rep. 2020;10(1):1–17.

[40] Yang W, Dicker DT, Chen J, et al. CARPs enhance p53 turnover by degrading 14-3-3σ and stabilizing MDM2. Cell Cycle. 2008;7 (5):670–682.

[41] Rowland AA, Chitwood PJ, Phillips MJ, et al. ER contact sites define the position and timing of endosome fission. Cell. 2014;159 (5):1027–1041.

[42] Shaner NC, Patterson GH, Davidson MW. Advances in fluorescent protein technology. J Cell Sci. 2007;120(24):4247–4260.

[43] Stewart SA, Dykxhoorn DM, Palliser D, et al. Lentivirus-delivered stable gene silencing by RNAi in primary cells. Rna. 2003;9 (4):493–501.

[44] Ran FA, Hsu PD, Wright J, et al. Genome engineering using the CRISPR-Cas9 system. Nat Protoc. 2013;8(11):2281–2308.

[45] Hammerling BC, Shires SE, Leon LJ, et al. Isolation of Rab5-positive endosomes reveals a new mitochondrial degradation pathway utilized by BNIP3 and Parkin. Small GTPases. 2020;11(1):69–76.

[46] Karbowski M, Neutzner A, Youle RJ. The mitochondrial E3 ubiquitin ligase MARCH5 is required for Drp1 dependent mitochondrial division. J Cell Biol. 2007;178(1):71–84.